The Cryosphere Discuss., 5, 1335–1364, 2011
www.the-cryosphere-discuss.net/5/1335/2011/
doi:10.5194/tcd-5-1335-2011

The Cryosphere Discussions

Warming of waters in an East Greenland fjord prior to glacier retreat: mechanisms and connection to large-scale atmospheric conditions

P. Christoffersen[1], **R. I. Mugford**[1,2], **K. J. Heywood**[3], **I. Joughin**[4], **J. A. Dowdeswell**[1], **J. P. M. Syvitski**[5], **A. Luckman**[6], **and T. J. Benham**[1]

[1]Scott Polar Research Institute, University of Cambridge, Cambridge, UK
[2]Environmental Systems Science Centre, University of Reading, Reading, UK
[3]School of Environmental Sciences, University of East Anglia, Norwich, UK
[4]Applied Physics Laboratory, University of Washington, Seattle, USA
[5]Institute of Arctic and Alpine Research, University of Colorado, Boulder, USA
[6]School of the Environment and Society, Swansea University, Swansea, UK

Received: 19 April 2011 – Accepted: 20 April 2011 – Published: 5 May 2011

Correspondence to: P. Christoffersen (pc350@cam.ac.uk)

Published by Copernicus Publications on behalf of the European Geosciences Union.

Abstract

Hydrographic data acquired in Kangerlugssuaq Fjord and adjacent seas in 1993 and 2004 are used together with ocean reanalysis to elucidate water mass change and ice-ocean-atmosphere interactions in East Greenland. The hydrographic data show substantial warming of fjord waters between 1993 and 2004 and warm subsurface conditions coincide with the rapid retreat of Kangerlugssuaq Glacier in 2004–2005. The ocean reanalysis shows that the warm properties of fjord waters in 2004 are related to a major peak in oceanic shoreward heat flux into a cross-shelf trough on the outer continental shelf. The heat flux into this trough varies according to seasonal exchanges with the atmosphere as well as from deep seasonal intrusions of subtropical waters. Both mechanisms contribute to high (low) shoreward heat flux when winds from the northeast are weak (strong). The combined effect of surface heating and inflow of subtropical waters is seen in the hydrographic data, which were collected after periods when along-shore coastal winds from the north were strong (1993) and weak (2004). We show that coastal winds vary according to the pressure gradient defined by a semi-permanent atmospheric pressure system over Greenland and a persistent atmospheric low situated near Iceland. The magnitude of this pressure gradient is controlled by longitudinal variability in the position of the Icelandic Low.

1 Introduction

The mass balance of the Greenland Ice Sheet has changed from a state with no apparent long term trend in the 1980s and 1990s (Rignot et al., 2008; Hanna et al., 2005) to a state where net annual losses can exceed 200 Gt yr^{-1} (Rignot and Kanagaratnam, 2006; Velicogna and Wahr, 2006; Chen et al., 2006; Rignot et al., 2008; van den Broeke et al., 2009). This ice loss is equivalent to a global sea-level rise of >0.6 mm a^{-1} and there is concern that future losses could accelerate substantially (IPCC, 2007). Up to 2/3 of a total net ice loss of 220 Gt in 2005 was caused by the acceleration of tidewater glaciers (Rignot and Kanagaratnam, 2006). Several large glaciers have subsequently slowed down, most notably Helheim Glacier and Kangerlugssuaq Glacier (henceforth referred to as KG) on the East Coast (Howat et al., 2007). However, van den Broeke et al. (2009) show that dynamic losses from discharge of ice into fjords still amount to ~50 % of the total net ice loss when the reduced discharges after 2005 are taken into account.

In recent years, nearly 75 % of the net annual imbalance from discharge has come from southeast Greenland (van den Broeke et al., 2009) where glacier fluctuations have been large and synchronous (Luckman et al., 2006; Stearns and Hamilton, 2007; Joughin et al., 2008; Howat et al., 2008). Whilst ice sheet surface melt is known to influence ice flow (Zwally et al., 2002) and cause diurnal fluctuations in flow speed (Shepherd et al., 2009), the effect of surface melt appears limited on interannual timescale (van de Wal et al., 2008; Sundal et al., 2011). The sustained increased in discharge of ice from eastern tidewater glaciers may therefore be related to oceanic conditions (Sole et al., 2008; Straneo et al., 2010; Seale et al., 2011).

Coastal waters in West Greenland have warmed since 1996 (Holland et al., 2008) and the warming may be related to increased transport of subtropical waters to the Irminger Sea (Falina et al., 2007; Sarafanov et al., 2007, 2009; Yashayaev et al., 2007). The latter occurred when the North Atlantic Oscillation (NAO) switched from a strong phase in 1993–1995 to a weak state in 1996, resulting in slowdown and contraction of the subpolar North Atlantic gyre (Flatau et al., 2003; Hakkinen and Rhines, 2004). As a consequence, warmer and larger volumes of subtropical waters entered the Irminger Sea and thus the Irminger Current, which splits near Denmark Strait. A small branch flows clockwise around Iceland while the larger branch flows southward along the East Greenland continental shelf edge (Fig. 1).

Although recent studies have suggested a sensitive interaction of the Greenland Ice Sheet with its surrounding seas (Holland et al., 2008; Rignot et al., 2010), ice-ocean interactions in Greenland remain uncertain and poorly documented. It is not yet clear if recent changes in the flow of tidewater glaciers were caused by increased transport of warm subtropical waters to coastal environments and fjords or by changes in the properties of these waters. The influence of air-sea heat exchange associated with sustained atmospheric warming, e.g. as reported by Box et al. (2009), is also not firmly established.

Here, we use hydrographic data acquired in Kangerlugssuaq Fjord (KFj) and adjacent seas in 1993 and 2004 together with an ocean reanalysis from the NEMO coupled sea-ice-ocean model to elucidate air-sea and ice-ocean interactions. The hydrographic datasets are unique in that they were acquired when the North Atlantic Oscillation (NAO) was strong (1993) and weak (2004), respectively, and the latter data were furthermore acquired during the early stage of the rapid and well-documented retreat of KG. In 1993, we found cold polar surface water (<0 °C) as well as strongly modified and relatively cold water with subtropical origin (∼1 °C or less). The subtropical waters extended further into the fjord in 2004 and the waters were less modified, warmer (∼1.8 °C or more) and located ∼100 m higher than in 1993, whilst polar surface water was up to 4 °C warmer than in 1993.

The reanalysis shows that oceanic heat flux directed towards KFj in 2003–2004 is several times higher than the heat flux of preceding years, and it peaks about one year prior to the abrupt retreat of KG. The heat flux varies according to seasonal heat exchange with the atmosphere as well as from deep seasonal inflows of subtropical waters onto the shelf. Both mechanisms contribute to high (low) shoreward heat flux when winds from the northeast are weak (strong) and warm (cold). The combined effect of surface heating and the deeper inflow of subtropical waters is consistent with the hydrographic data, which was collected after periods when northerly winds were strong (1993) and weak (2004).

TCD
5, 1335–1364, 2011

2 Data and methods

2.1 Hydrographic surveys

Hydrographic data from KFj and from transects along the submarine trough known as Kangerlugssuaq trough (KTr) were acquired during 4–16 September 1993 and 1–10 September 2004 (Fig. 1a). A Sea-Bird 19 with conductivity, temperature and depth (CTD) sensor was used in 1993 to derive salinity and potential temperature at five stations along KTr, from the mouth of KFj to the continental shelf break (Fig. 1a), and in three stations located in the central upper part of the fjord near KG (Fig. 3a) (Azetsu-Scott and Tan, 1997). In 2004, we repeated as far as icebergs allowed the station locations occupied by Azetsu-Scott and Tan (1997), using a Sea-Bird 911 plus CTD sensor to derive salinity and potential temperature. The difference in station locations in the upper part of KFj (Fig. 3a) was a result of high concentration of icebergs produced by KG in July and August 2004, during the early phase of the prolonged retreat that lasted until March 2005. Salinity and temperature sensors were calibrated prior to data acquisition. Salinity was further calibrated in 2004 using salinity samples collected at each station from the rosette water sampler mounted on the CTD frame. The bathymetry of KFj and the adjacent East Greenland shelf and its cross-shelf trough (KTr) are from Syvitski et al. (1996) and Dowdeswell et al. (2010).

2.2 Ocean reanalysis

The interannual variations of subsurface waters along the East Greenland continental shelf were examined using a 22-yr-long ocean reanalysis (1987–2008) from the NEMO coupled sea-ice-ocean model version 2.3 (Madec, 2008). The reanalysis was produced by the OPA9 ocean model and the LIM2.0 sea ice model (Fichefet and Maqueda, 1997; Goosse and Fichefet, 1999) with eddy-permitting 1/4° resolution on the tripolar ORCA025 grid (Barnier et al., 2006). Hydrographic data were assimilated using the $S(T)$ method (Haines et al., 2006). The OPA9 ocean model is a primitive equation z-level model, using hydrostatic and Boussinesq approximations. The model applies a linearised free-surface and the bottom topography is discretised as partial steps (Adcroft et al., 1997). There are 46 vertical levels, with thicknesses ranging from 6 m at the surface to 250 m at the ocean floor. The deep (>300 m) bathymetry at 1/4° resolution was constructed from the 2-min ETOPO global bathymetric field from the National Geophysical Data Centre, NOAA, while shallower regions on the continental shelves between 88° S and 88° N was approximated with the GEBCO 1-min bathymetry.

Surface atmospheric forcing for the reanalysis is the DRAKKAR Forcing Set 3 (Brodeau et al., 2010), a hybrid dataset making use of the ERA-40 atmospheric reanalysis, ECWMF operational analyses and the Common Ocean Reference Experiment dataset (Large and Yeager, 2004). The parameter settings of the eddy-permitting 1/4° resolution NEMO ocean model are discussed by Barnier et al. (2006) and Penduff et al. (2010).

The model experiment used for this analysis is referred to as UR025.1. In situ temperature and salinity observations were assimilated from the UK Met Office quality controlled ENACT/ENSEMBLES dataset EN3-v1c, which includes data from the World Ocean Database 2005 (http://www.nodc.noaa.gov/OC5/WOD05/pr_wod05.html), the Global Temperature-Salinity Profile Program (http://www.nodc.noaa.gov/GTSPP/) and Argo (http://www.argo.net). There is good coverage of temperature and salinity observations in the EN3-v1c dataset off the coast of East Greenland and the Irminger Sea, which is the area of interest in this study (Fig. 2). The assimilation of hydrographic data in UR025.1 limits model bias and results in more accurate representation of water mass properties, leading to a simulation where outputs are consistent with independent hydrographic observations (Gemmell et al., 2008, 2009; Smith et al., 2010). The correction of density gradients furthermore improves the circulation. It is therefore appropriate to utilise UR025.1 to investigate changes in temperature and salinity of waters off the East Coast of Greenland. The performance of UR025.1 in terms of water mass properties and circulation in the Arctic Ocean, where the extent of hydrographic observations is more limited than in the subpolar North Atlantic, is discussed by Zuo et al. (2011).

3 Results

3.1 Hydrographic observations from KFj and KTr

We identify four different water masses with properties similar to those characterised by Rudels et al. (2002) and Sutherland and Pickart (2008). In 1993, Atlantic Water (AW) with potential temperature $\theta > 2\,^{\circ}$C and salinity $S \sim 35$ penetrated beneath cold Polar Surface Water (PSW) with $\theta < 0\,^{\circ}$C and $S < 32$ (Fig. 1b). The densest water on the shelf was Polar Intermediate Water (PIW) with potential density of $\sigma_\theta > 27.9$ compared with $27.55 < \sigma_\theta < 27.75$ for AW and $\sigma_\theta < 27.7$ for PSW. Inside KFj (Fig. 3), we observed cold PSW ($\theta \sim -1\,^{\circ}$C) in the upper 100 m while deeper water was the denser PIW (Fig. 3a). Cooled and strongly modified AW water (~1 °C or less) was located near the fjord mouth at 280–590 m depth (Fig. 3c, e) and at depths >350 m in the central part of the fjord (Fig. 3b, d). Warm PSW (PSWw) with $\theta > 2\,^{\circ}$C and $S < 32$ was in 2004 present throughout the 300-km-long shelf (Fig. 1c). The PSWw inside the fjord was up to 4 °C warmer than the PSW observed in 1993 (Fig. 3b, d). The temperature of PSWw near the fjord mouth was >3 °C in 2004 compared with <0 °C for PSW in 1993 (Fig. 3c, e). The AW deep intrusion was in 2004 warmer (1.8 °C) and located 100 m higher than in 1993 (Fig. 3d, e).

Figure 4 shows mean annual air temperature in Aputiteq at the southern end of the fjord mouth (67.78° N, 32.30° W, 25 m above sea level). The record shows that air temperatures during the early 2000s were considerably warmer than the 1990s. The mean annual air temperature was −2.4 °C in 2004 compared to −4.4 °C in 1993. The mean temperature averaged for summer months only (June–September) was 2.8 °C in 2004 compared to 0.90 °C in 1993. The θ-S plots in Fig. 3 nonetheless show that properties of PSWw observed in 2004 were influenced by mixing with warm AW in addition to the exchange of heat with the atmosphere. However, with only two snapshots of the subsurface conditions, we cannot firmly establish whether the measured properties represent a significant change or whether they are a result of seasonal or

TCD
5, 1335–1364, 2011

higher frequency variability. The properties of water masses in the intervening period are therefore examined using the ocean reanalysis described in Sect. 2.2 above.

3.2 Shelf water exchange

The KTr is a cross-shelf trough, extending about 300 km from the fjord mouth to the continental shelf edge. It has a maximum depth of about 600 m set between shallower banks of about 400 m water depth (Syvitski et al., 1996; Dowdeswell et al., 2010). The trough is capable of steering waters in the East Greenland and Irminger currents onto the continental shelf, as illustrated in Fig. 1a (Sutherland and Pickart, 2008). Figure 5 shows Hovmøller diagrams of temperature and salinity for water masses flowing into and out of KTr (see Fig. 2 for location). Seasonal changes are seen at all depths with near-surface temperatures varying between ∼0 °C in winter to ∼10 °C in summer. Decadal averages of temperature (salinity) of surface waters (upper 100 m) change from 4.5 °C (34.54) in 1989–1998 to 5.6 °C (34.70) in 1999–2008 (Fig. 6a). This trend comprises a gradual rise from 3.3 °C (34.38) in 1995 to 6.9 °C (34.87) in 2003. The seasonal temperature changes at depths of 400–800 m are not caused by near-surface variations related to sea ice formation and melt and the exchange of heat with the atmosphere (Fig. 5). The variations are caused instead by movement of water masses onto and off the continental shelf, with temperature and salinity of deep waters co-varying synchronously (Fig. 6a, b). Decadal averages of temperature (salinity) at 400–800 m rise from 4.1 °C (34.98) in 1989–1998 to 4.7 °C (35.03) in 1999–2008. The increases in temperature and salinity are higher than the warming (∼0.2 °C) and salinification (∼0.022) observed in the central Irminger Sea at equivalent depth between 1996 and 2006 (Sarafanov et al., 2007). The difference is related to the variable volume flux of AW into KTr. Notable increase in the inflow of AW occurred in 1991, 1996 and 2001–2005 (Fig. 6a, b), corresponding to years when the NAO was weak. The extended NAO winter index (December–March), which is based on the difference of normalised sea-level pressure between Lisbon (Portugal) and Stykkisholmur (Iceland), is shown in Fig. 6b. The index has a marked similarity to salinity as well as temperature variations at 400–800 m (Fig. 6a). This connection is related to coastal winds, as explained in Sect. 5 below, whilst changing properties of surface water is mainly a result of increased air-sea heat exchange due to warm atmospheric conditions in 1995–2005 (Chylek et al., 2006; Box et al., 2009). The latter is also seen in the Aputiteq temperature record (Fig. 4). The increased temperatures near the surface as well as depths of 400–800 m cause high heat flux into KTr in 2003–2004 (Fig. 6c). The heat flux with reference to 0 °C is calculated across the transect shown in Fig. 1a. Although the value of this flux is not definitive, as it is calculated on the basis of a reference value and because there is a net volume flux across the transect, its relative temporal variability is both meaningful and informative. The inter-annual trend of the heat flux into KTr, as shown in Fig. 6c, is calculated by filtering monthly mean values with a 12-month-moving average. The heat flux varies significantly with peaks and troughs ranging from 2.8 TW in 1994 to 13 TW in 2003 and back to 3.2 TW in 2007. This variability is a result of variable air-sea heat exchange as well as variable extent of intrusions of AW onto the shelf. However, the mean annual heat flux was <5 TW in 1992–1995 while >11 TW in 2003–2004. It then decreased to <6 TW in 2005–2008.

Figure 7 shows correlations between volume and heat fluxes into KTr and atmospheric forcing. The volume flux (positive north, i.e. into KTr) correlates with the wind speed across Denmark Strait at 66.3° N (Fig. 7a). Correlation coefficients are $r = 0.69$ for winter months (December to March) and $r = 0.61$ when all data are included. Heat flux into KTr is strongly correlated with volume flux into KTr (Fig. 7b) ($r = 0.85$), which is not surprising because the former is calculated from the latter. However, we also find that the volume flux into KTr correlates strongly with along-shore volume flux ($r = 0.74$) (Fig. 7c). This shows that strong (weak) along-shore transport coincides with low (high) volume and heat fluxes into KTr and this is due to the strong (weak) forcing by coastal winds.

TCD
5, 1335–1364, 2011

Surface atmospheric forcing used to drive the ocean model is illustrated in Fig. 8. In the winter of 1994–1995, northerly winds are persistently strong (Fig. 8a). These winds cool surface waters and increase the transport of water masses along the coast (Bacon et al., 2008). Cold and fresh waters flow out of KTr as a result, and this reduces the inflow of AW. 1994–1995 is the only winter where the calculated heat flux into KTr is negative from December to March (Fig. 7). Atmospheric conditions are fundamentally different in the winter of 1995–1996 when northerly winds were uncharacteristically and persistently weak (Fig. 8b). This change of atmospheric conditions is seen in the meteorological record from Aputiteq where mean winter air temperature (December–March) in 2004–2005 is $-8.7\,^{\circ}$C compared to $-11.7\,^{\circ}$C in the previous winter (Fig. 4). The ocean model shows that transportation of cold water masses out of KTr is concurrently reduced while inflow of AW is substantially increased (Fig. 5). Whilst air-sea interactions are considerably different in 1995 and 1996, a prolonged warm phase associated with reduced air flow through Denmark Strait occur in 2001–2005. This results in high and persistent inflow of AW at depths of 400–800 m while surface waters warm due to exchange of heat with the atmosphere (Fig. 5). The heat flux directed into KTr is in 2003 and 2004 therefore about threefold that of the early 1990s (Fig. 6c). Cold and relatively strong air flow from northeast re-occur after 2005 and inflows of AW and the heat flux into KTr return to levels similar to those in the early 1990s (Fig. 6c).

4 The abrupt retreat of KG in 2004–2005

Figure 6c shows the calculated heat flux into KTr as well as mean monthly calving-front position of KG. The front positions ($n = 760$) are determined from MODIS imagery acquired since 2000 and as described by Seale et al. (2011). The time series was extended using previously published data for 1992–2000 (Luckman et al., 2006). An interannual trend is derived by eliminating the seasonal variability and this was done by filtering monthly mean positions with a 12-month moving average. This trend is defined by advance of ∼1.5 km in 1992–1995; retreat of ∼3 km in 1996–1998; relatively

TCD
5, 1335–1364, 2011

constant positions between 1999 and 2004; and a sudden large retreat of >5 km between July 2004 and March 2005, as described in several previous studies (Howat et al., 2007; Joughin et al., 2008; Luckman et al., 2006; Stearns and Hamilton, 2007). The glacier re-advanced ~2 km in 2006–2007 and variation has since been restricted to regular seasonal fluctuations. The large retreat in 2004–2005 is well-documented by MODIS imagery, which shows retreat of 2.2 km between 1 July and 14 September 2004, which was when the latest set of hydrographic data shown in Fig. 3 were acquired. Large amounts of icebergs were present in the fjord during the cruise in 2004 and the MODIS imagery shows that this condition was caused by break-up of the sikussak (a seasonally rigid melange of icebergs, bergy bits and sea ice) in front of KG. Contrary to previous years, recession continued throughout autumn and winter, with the calving front located 6.8 km inland of the 2004 maximum position on 8 March 2005 (Joughin et al., 2008; Seale et al., 2011).

The time series of heat flux into KTr and the observed margin position of KG show that the rapid retreat in 2004–2005 occurred about one year after the peak heat flux in the ocean reanalysis. This delay is comparable to transportation of AW across the shelf, although we do not know how accurately the eddy-permitting model simulates across shelf flows. Nonetheless, the shelf waters including AW were in September 2004 observed to flow at rates up to 20 cm s^{-1} across the station transect shown in Fig. 1a, suggesting the transport of AW from continental slope to fjord is feasible in one year or less. Transport of AW from fjord mouth to glacier termini may require only a few weeks if the circulation of water masses is influenced by intermittent storms, as reported by Straneo et al. (2010) for the similarly sized Sermilik Fjord farther south.

5 Synoptic atmospheric forcing

Our results show that coastal wind forcing in East Greenland is related to the large-scale atmospheric pressure gradient across Denmark Strait. Here, we define the latter, ΔP, as the difference between weather station measurements in Stykkishólmur

(Iceland) and Tasiilaq (East Greenland), and its relation to wind forcing is shown in Fig. 7d. There is a strong correlation between ΔP and wind speed ($r = 0.87$) because the former is a very good indicator of the geostrophic wind, developing from a stationary atmospheric high-pressure system residing over the Greenland Ice Sheet and the Icelandic Low (IL) (Blindheim and Malmberg, 2005; Bacon et al., 2008). The IL is a synoptic pressure system that defines the northern component of the NAO. The geostrophic wind represented by highly negative ΔP (about −5 hPa) is strong and cold, and the air flow follows the coast from the northeast. This wind pattern develops when a deep IL and the stable high pressure over Greenland result in isobars that are near-parallel to the East Coast of Greenland (Bacon et al., 2008). Northerly winds are weak when ΔP approaches or exceeds zero, as it did in 1996 and in the early 2000s, when the IL was positioned differently. The prevailing wind in this setting is warmer and directed towards shore because isobars are perpendicular to the coast. The connection between the large-scale pressure systems and prevailing wind is seen in Fig. 4 as a statistically significant relationship between ΔP and the mean annual air temperature in Aputiteq. Below, we refer to highly negative values of ΔP as high ΔP while values near zero and above are referred to as low ΔP.

The link between ΔP and the IL is found when the latter is considered to be a "centre of action". Bakalian et al. (2007) used "centres of action", as defined by Hameed et al. (1995), to show that the latitude of the IL influences the frequency of intermittent storms known as tip jets. Adopting the same technique, we determine the latitude and longitude of the IL using monthly mean sea level pressure data in the ERA-Interim reanalysis, which cover our period of investigation (Simmons et al., 2006). An area-weighted departure from a sea-level pressure threshold of 1014 mb is in this approach calculated for December to March in a domain that encircles 45° N to 70° N and 70° W to 10° E. Variations in the latitude and longitude of IL are shown in Fig. 9 together with the NAO winter index (Fig. 9a) and ΔP (Fig. 9b). The data show a strong statistical correlation between (i) the latitude of IL and the NAO index ($r = 0.78$), and (ii) the longitude of IL and ΔP ($r = 0.82$). The first relationship shows that the IL has a northern

TCD
5, 1335–1364, 2011

Warming of waters in an East Greenland fjord prior to glacier retreat

P. Christoffersen et al.

(southern) position when the NAO index is high (low). The second shows that periods of high (low) ΔP, corresponding to strong (weak) northeasterly air flow in East Greenland, occur when the IL has an eastern (western) position. The eastern position of the IL is over the Irminger Sea southwest of Iceland (~32–35° W), whereas the western position is over the Labrador Sea closer to Canada (~39–42° W). Almost identical relationships are found in ERA-40, which is a reanalysis product of the ECMWF covering the period 1958–2002 (Uppala et al., 2005). The correlations are $r \geq 0.99$ when IL positions for the period of overlap (1989–2002) are compared. Furthermore, the relationships between IL position, NAO index and ΔP remain statistically significant on the 99 % level when ERA-40 reanalysis data for 1958–1988 are used together with the ERA-Interim reanalysis (1989–present). The relationships are also seen in the NCEP/NCAR reanalysis data (Kalnay et al., 1996) (data not shown), confirming that the interannual variability of the IL as a centre of action can be firmly identified with atmospheric reanalysis data.

6 Synthesis

A switch of the IL from 31.6° W in the winter of 1994–1995 to 41.4° W in 1995–1996 (Fig. 9) and the accompanying change of ΔP from −4.5 hPa to +2.2 hPa (Fig. 4) explains the very different wind forcing fields shown in Fig. 8. The switch from strong to weak northeasterly air flow warms the surface layer at KTr, while deeper levels warm from the concurrent higher inflow of AW at depth. Although the ocean reanalysis was produced with assimilation of extensive hydrographic data including the Irminger Sea, constraints from the seasonally ice covered coastal regions are more sparse, so we cannot firmly establish the transportation of AW inside and around fjords. Nonetheless, the warming and cooling of coastal waters seen in the reanalysis at the outer continental shelf is consistent with observations. Holland et al. (2008) show that AW from the Irminger Sea and the East Coast warmed coastal waters in West Greenland after 1997 and they suggest that the warming was a result of a the shift in the NAO from

TCD
5, 1335–1364, 2011

a very strong phase in 1992–1995 to a very weak state in 1996. Warming associated with this event is clearly seen in the ocean reanalysis, and we attribute the warming to primarily be a result of the change in ΔP and the coastal winds. The warming in 1996 may be the cause of substantial thinning of KG by 50 m at some point between 1993 and 1998 (Thomas et al., 2000). The thinning reported by Thomas et al. (2000) coincides with our observed interannual retreat of ~3 km in 1995–1998 (Fig. 6c), which is significant because seasonal variability is excluded, although considerably less than the retreat experienced by the glacier in 2004–2005. The larger impact of the latter event is explained in our analysis by surface warming as well as a higher inflow of subtropical waters at depth. The concurrent warming of surface waters and the deeper inflows of AW is consistent with the hydrographic data from KFj and both aspects of warming were a result of weak northeasterly air flow associated with low ΔP and a persistent eastern position of the IL over the Labrador Sea (Fig. 9b).

7 Summary and conclusions

Hydrographic surveys conducted in KFj and in transects along KTr show significant warming of PSW as well as increased inflow of AW between 1993 and 2004. In 1993, we found strongly modified and relatively cold (~1 °C or less) water with subtropical origin at depths at 280–590 m depth near coast and at depths >350 m in the central part of the fjord. The subtropical waters extended further into the fjord in 2004 and the waters were less modified, warmer (~1.8 °C or more) and located ~100 m higher than in 1993. The surface layer changed from cold (< −1 °C) PSW in 1993 to much warmer PSWw (>2 °C) in 2004, consistent with a change in mean air temperature for June–September from 0.90 °C in 1993 to 2.8 °C in 2004. Surface warming and AW inflows at depth are both important. The former may have delayed the onset of seasonal freeze-up, whilst promoting continued retreat of KG, as observed (Fig. 6c), due to delayed freeze-up and a subsequently prolonged season with open water and high calving rate. The latter would have influenced KG directly if AW was in direct contact with the calving front, but we cannot confirm this with the available data.

TCD
5, 1335–1364, 2011

Subtropical waters in an ocean reanalysis is found to seasonally intrude into KTr, a glacially eroded cross-shelf submarine trough extending from KFj to the continental shelf edge. The intrusions occur mainly in spring and early summer and at a depth of several hundred meters, and they are driven by winds. Thoma et al. (2008) report similar wind-driven intrusions into a trough carved by glaciers on the Amundsen Sea continental shelf in Antarctica. The oceanic forcing of East Greenland tidewater glaciers may thus be similar to the oceanic forcing of ice streams in the Amundsen Sea Embayment, although the former are associated with a much faster response due to their smaller size and much steeper terrain (see analysis in Howat et al. (2005) for a comparison). The along-shore volume and freshwater fluxes increase when northerly winds are strong while towards-shore volume and heat fluxes into KTr are reduced or even negative. When northerly winds are weak, surface waters warm due to warmer easterly air flow. Deep waters warm because subtropical waters flows onto the shelf at depths >400 m. We calculated the annual heat flux into KTr and there is significant variations: from <5 TW in 1992–1995 to >11 TW in 2003–2004. The heat flux was much reduced in 2005–2008 with values ranging from 4.4 TW to 6.1 TW and this decrease coincide with the stabilisation and partial re-advance of KG in 2005–2008. The hydrographic station data from KTr show transport of water masses across the shelf at rates of 1–10 $\mathrm{cm\,s^{-1}}$, suggesting that advection of AW from continental slope to fjord may occur in one year or less. If AW is subsequently flushed through the fjord by the intermediary circulation described by Straneo et al. (2010), KG could be exposed to subtropical AW very effectively. A previously documented episode of thinning in the mid-1990s coincide with observed retreat of KG by ~3 km and with a sudden warming of waters on the outer shelf in 1996 due to a major shift in the intensity of the NAO. We show that this event caused sudden warming of coastal waters due to a marked change of winds on synoptic scale and that it was a precursor of the larger event in 2004–2005.

The results from this study show that the seasonal and large-scale characteristics of coastal winds are controlling factors in exchange of water masses off the coast of

East Greenland. The wind stress on a synoptic scale is defined by the direction and magnitude of isobars associated with semi-permanent atmospheric pressure systems residing over Greenland (high pressure) and near Iceland (low pressure). We found that variations in the longitudinal position of the IL explain 67 % of the variability in ΔP, which is the atmospheric pressure gradient that controls the wind stress along the East Coast of Greenland. The wind stress is high and from the north when the IL is positioned over the Irminger Sea (~35° W) and this synoptic setting is associated with cold air temperatures and cooling of coastal water masses. The wind stress is low and from the east when the IL is situated over the Labrador Sea (~40° W) and this synoptic setting is associated with warmer air flow and warming of cooling of coastal water masses. The geostrophic wind should therefore be regarded as a key factor in the oceanographic forcing of the Greenland Ice Sheet.

Acknowledgements. The cruise to Kangerlugssuaq Fjord in 1993 was funded by the Geological Survey of Canada and the National Science Foundation (USA). The cruise in 2004 was funded by the Natural Environment Research Council. The ocean reanalysis was produced in the IPY ASBO programme funded by the Natural Environment Research Council. We are grateful to the crew and staff on the C. S. S. Hudson (1993) and the James Clark Ross (2004). R. M. thanks Keith Haines and Greg Smith for their help with the NEMO ocean model.

References

Adcroft, A., Hill, C., and Marshall, J.: Representation of topography by shaved cells in a height coordinate ocean model, Mon. Weather Rev., 125, 2293–2315, 1997.

AzetsuScott, K. and Tan, F. C.: Oxygen isotope studies from Iceland to an East Greenland Fjord: Behaviour of glacial meltwater plume, Mar. Chem., 56, 239–251, 1997.

Bacon, S., Myers, P. G., Rudels, B., and Sutherland, D. A.: Accessing the inaccessible: Buoyancy-driven coastal currents on the shelves of Greenland and eastern Canada, in: Arctic-Subarctic Ocean Fluxes, edited by: Dickson, R. R., Meincke, J., and Rhines, P., Springer, Dordrecht, 703–722, 2008.

TCD

5, 1335–1364, 2011

Blindheim, J. and Malmberg, S. A.: The mean sea level pressure gradient across the Denmark Strait as an indicator of conditions in the North Icelandic Irminger current, in: The Nordic Seas: An Integrated Perspective, American Geophysical Union, Geophysical Monograph Series, edited by: Drange, H., Dokken, T., Furevik, T., Gerdes, R., and Berger, W., Geophysical Monograph Series, American Geophysical Union, 65–71, 2005.

Box, J. E., Yang, L., Bromwich, D. H., and Bai, L. S.: Greenland Ice Sheet Surface Air Temperature Variability: 1840–2007, J. Climate, 22, 4029–4049, 2009.

Brodeau, L., Barnier, B., Treguier, A. M., Penduff, T., and Gulev, S.: An ERA40-based atmospheric forcing for global ocean circulation models, Ocean Model., 31, 88–104, 2010.

Chen, J. L., Wilson, C. R., and Tapley, B. D.: Satellite gravity measurements confirm accelerated melting of Greenland ice sheet, Science, 313, 1958–1960, doi:10.1126/science.1129007, 2006.

Chylek, P., Dubey, M. K., and Lesins, G.: Greenland warming of 1920–1930 and 1995–2005, Geophys. Res. Lett., 33, L11707, doi:10.1029/2006gl026510, 2006.

Dowdeswell, J. A., Evans, J., and Ó Cofaigh, C.: Submarine landforms and shallow acoustic stratigraphy of a 400 km-long fjord-shelf-slope-transect, Kangerlussuaq margin, East Greenland, Quaternary Sci. Rev., 29, 3359–3369, 2010.

Falina, A., Sarafanov, A., and Sokov, A.: Variability and renewal of Labrador Sea Water in the Irminger Basin in 1991–2004, J. Geophys. Res., 112, C01006, doi:10.1029/2005jc003348, 2007.

Fichefet, T. and Maqueda, M. A. M.: Sensitivity of a global sea ice model to the treatment of ice thermodynamics and dynamics, J. Geophys. Res.-Oceans, 102, 12609–12646, 1997.

Flatau, M. K., Talley, L., and Niiler, P. P.: The North Atlantic Oscillation, surface current velocities, and SST changes in the subpolar North Atlantic, J. Climate, 16, 2355–2369, 2003.

Gemmell, A., Smith, G. C., Haines, K., and Blower, J. D.: Evaluation of water masses in ocean synthesis products, CLIVAR Exchanges, 13, 7–9, 2008.

Gemmell, A., Smith, G. C., Haines, K., and Blower, J. D.: Ocean model-data analyses with Ocean DIVA, Journal of Operational Oceanography, 2, 29–41, 2009.

Goosse, H. and Fichefet, T.: Importance of ice-ocean interactions for the global ocean circulation: A model study, J. Geophys. Res.-Oceans, 104, 23337–23355, 1999.

Haines, K., Blower, J. D., Drecourt, J. P., Liu, C., Vidard, A., Astin, I., and Zhou, X.: Salinity assimilation using S(T): Covariance relationships, Mon. Weather Rev., 134, 759–771, 2006.

Hakkinen, S. and Rhines, P. B.: Decline of subpolar North Atlantic circulation during the 1990s,

Science, 304, 555–559, 2004.
Hameed, S., Shi, W., Boyle, J., and Santer, B.: Investigation of the centers of action in the North Atlantic and North Pacific in the ECHAM AMIP simulation, Proceeding of the First International AMIP Scientific Conference, p. 78, 1995.
Hanna, E., Huybrechts, P., Janssens, I., Cappelen, J., Steffen, K., and Stephens, A.: Runoff and mass balance of the Greenland ice sheet: 1958–2003, J. Geophys. Res.-Atmos., 110, D13108, doi:10.1029/2004jd005641, 2005.
Holland, D. M., Thomas, R. H., de Young, Ribergaard, M. H., and Lyberth, B.: Acceleration of Jakoshavn Isbrae triggered by warm susurface ocean waters, Nat. Geosci., 1, 659–664, 2008.
Howat, I. M., Joughin, I., Tulaczyk, S., and Gogineni, S.: Rapid retreat and acceleration of Helheim Glacier, east Greenland, Geophys. Res. Lett., 32, L22502, doi:10.1029/2005GL024737, 2005.
Howat, I. M., Joughin, I., and Scambos, T. A.: Rapid changes in ice discharge from Greenland outlet glaciers, Science, 315, 1559–1561, 2007.
Howat, I. M., Joughin, I., Fahnestock, M., Smith, B. E., and Scambos, T. A.: Synchronous retreat and acceleration of southeast Greenland outlet glaciers 2000–2006: ice dynamics and coupling to climate, J. Glaciol., 54, 646–660, 2008.
IPCC: Climate change 2007: The Physical Science Basis. Contributions of Working Group 1 to the Fourth Assessment Report of the Intergovernmental Panel on Climate Change, edited by: Solomon, S., Qin, D., Manning, M., Chen, Z., Marquis, M., Averyt, K. B., Tignor, M., and Miller, H. L., Cambridge University Press, Cambridge, UK, and New York, USA, 996 pp., 2007.
Joughin, I., Howat, I., Alley, R. B., Ekstrom, G., Fahnestock, M., Moon, T., Nettles, M., Truffer, M., and Tsai, V. C.: Ice-front variation and tidewater behavior on Helheim and Kangerdlugssuaq Glaciers, Greenland, J. Geophys. Res., 113, F01004, doi:10.1029/2007jf000837, 2008
Kalnay, E., Kanamitsu, M., Kistler, R., Collins, W., Deaven, D., Gandin, L., Iredell, M., Saha, S., White, G., Woollen, J., Zhu, Y., Chelliah, M., Ebisuzaki, W., Higgins, W., Janowiak, J., Mo, K. C., Ropelewski, C., Wang, J., Leetmaa, A., Reynolds, R., Jenne, R., and Joseph, D.: The NCEP/NCAR 40-year reanalysis project, B. Am. Meteorol. Soc., 77, 437–471, 1996.
Large, W. G. and Yeager, S. G.: Diurnal to decadal global forcing for ocean and sea-ice models: The data sets and flux climatologies, Technical Report, TN-460+STR, The National Center

TCD
5, 1335–1364, 2011

Warming of waters in an East Greenland fjord prior to glacier retreat

P. Christoffersen et al.

for Atmospheric Research, 105 pp., 2004.
Luckman, A., Murray, T., de Lange, R., and Hanna, E.: Rapid and synchronous ice-dynamic changes in East Greenland, Geophys. Res. Lett., 33, L03503, doi:10.1029/2005GL025428, 2006.
Madec, G.: NEMO reference manual, ocean dynamics component: NEMO-OPA. , Institut Pierre-Simon Laplace (IPSL), Paris, 2008.
Rignot, E. and Kanagaratnam, P.: Changes in the velocity structure of the Greenland ice sheet, Science, 311, 986–990, 2006.
Rignot, E., Braaten, D., Gogineni, S. P., Krabill, W. B., and McConnell, J. R.: Rapid ice discharge from southeast Greenland glaciers, Geophys. Res. Lett., 31, L10401, doi:10.1029/2004GL019474, 2004.
Rignot, E., Box, J. E., Burgess, E., and Hanna, E.: Mass balance of the Greenland ice sheet from 1958 to 2007, Geophys. Res. Lett., 35, L20502, doi:10.1029/2008gl035417, 2008.
Rignot, E., Koppes, M., and Velicogna, I.: Rapid submarine melting of the calving faces of West Greenland glaciers, Nat. Geosci., 3, 187–191, 2010.
Rudels, B., Fahrbach, E., Meincke, J., Budeus, G., and Eriksson, P.: The East Greenland Current and its contribution to the Denmark Strait overflow, ICES J. Mar. Sci., 59, 1133–1154, 2002.
Sarafanov, A., Sokov, A., Demidov, A., and Falina, A.: Warming and salinification of intermediate and deep waters in the Irminger Sea and Iceland Basin in 1997–2006, Geophys. Res. Lett., 34, L23609, doi:10.1029/2007gl031074, 2007.
Sarafanov, A., Falina, A., Mercier, H., Lherminier, P., and Sokov, A.: Recent changes in the Greenland-Scotland overflow-derived water transport inferred from hydrographic observations in the southern Irminger Sea, Geophys. Res. Lett., 36, L13606, doi:10.1029/2009gl038385, 2009.
Seale, A., Christoffersen, P., Mugford, R. I., and O'Leary, M.: Ocean forcing of the Greenland Ice Sheet: Calving fronts and patterns of retreat identified by automatic satellite monitoring of eastern outlet glaciers, J. Geophys. Res.-Earth, accepted, 2011.
Shepherd, A., Hubbard, A., Nienow, P., King, M., McMillan, M., and Joughin, I.: Greenland ice sheet motion coupled with daily melting in late summer, Geophys. Res. Lett., 36, L01501, doi:10.1029/2008gl035758, 2009.
Simmons, A., Uppsala, S., Dee, D., and Kobayashi, S.: ERA-Interim: New ECMWF reanalysis products from 1989 onwards, European Centre for Medium-Range Weather Forecasts

Newsletter, 110, 25–35, 2006.
Smith, G. C., Haines, K., Kanzow, T., and Cunningham, S.: Impact of hydrographic data assimilation on the modelled Atlantic meridional overturning circulation, Ocean Sci., 6, 761–774, doi:10.5194/os-6-761-2010, 2010.
Sole, A., Payne, T., Bamber, J., Nienow, P., and Krabill, W.: Testing hypotheses of the cause of peripheral thinning of the Greenland Ice Sheet: is land-terminating ice thinning at anomalously high rates?, The Cryosphere, 2, 205–218, doi:10.5194/tc-2-205-2008, 2008.
Stearns, L. A. and Hamilton, G. S.: Rapid volume loss from two East Greenland outlet glaciers quantified using repeat stereo satellite imagery, Geophys. Res. Lett., 34(5), L05503, doi:10.1029/2006gl028982, 2007.
Straneo, F., Hamilton, G. S., Sutherland, D. A., Stearns, L. A., Davidson, F., Hammill, M. O., Stenson, G. B., and Rosing-Asvid, A.: Rapid circulation of warm subtropical waters in a major glacial fjord in East Greenland, Nat. Geosci., 3, 182–186, 2010.
Sundal, A. V., Shepherd, A., Nienow, P., Hanna, E., Palmer, S., and Huybrechts, P.: Melt-induced speed-up of Greenland ice sheet offset by efficient subglacial drainage, Nature, 469, 521–524, 2011.
Sutherland, D. A. and Pickart, R. S.: The East Greenland Coastal Current: Structure, variability, and forcing, Prog. Phys. Oceanogr., 78, 58–77, 2008.
Syvitski, J. P. M., Andrews, J. T., and Dowdeswell, J. A.: Sediment deposition in an iceberg-dominated glacimarine environment, East Greenland: Basin fill implications, Global Planet. Change, 12, 251–270, 1996.
Thoma, M., Jenkins, A., Holland, D., and Jacobs, S.: Modelling Circumpolar Deep Water intrusions on the Amundsen Sea continental shelf, Antarctica, Geophys. Res. Lett., 35, L18602, doi:10.1029/2008gl034939, 2008.
Thomas, R. H., Abdalati, W., Akins, T. L., Csatho, B. M., Frederick, E. B., Gogineni, S. P., Krabill, W. B., Manizade, S. S., and Rignot, E. J.: Substantial thinning of a major east Greenland outlet glacier, Geophys. Res. Lett., 27, 1291–1294, 2000.
Uppala, S. M., Kallberg, P. W., Simmons, A. J., Andrae, U., Bechtold, V. D., Fiorino, M., Gibson, J. K., Haseler, J., Hernandez, A., Kelly, G. A., Li, X., Onogi, K., Saarinen, S., Sokka, N., Allan, R. P., Andersson, E., Arpe, K., Balmaseda, M. A., Beljaars, A. C. M., Van De Berg, L., Bidlot, J., Bormann, N., Caires, S., Chevallier, F., Dethof, A., Dragosavac, M., Fisher, M., Fuentes, M., Hagemann, S., Holm, E., Hoskins, B. J., Isaksen, L., Janssen, P., Jenne, R., McNally, A. P., Mahfouf, J. F., Morcrette, J. J., Rayner, N. A., Saunders, R. W., Simon, P.,

TCD
5, 1335–1364, 2011

Warming of waters in an East Greenland fjord prior to glacier retreat

P. Christoffersen et al.

Sterl, A., Trenberth, K. E., Untch, A., Vasiljevic, D., Viterbo, P., and Woollen, J.: The ERA-40 re-analysis, Q. J. Roy. Meteor. Soc., 131, 2961–3012, 2005.

van de Wal, R. S. W., Boot, W., van den Broeke, M. R., Smeets, C. J. P. P., Reijmer, C. H., Donker, J. J. A., and Qoerlemans, J.: Large and rapid melt-induced velocity changes in the Ablation zone of the Greenland Ice Sheet, Science, 321, 111–113, 2008.

van den Broeke, M., Bamber, J., Ettema, J., Rignot, E., Schrama, E., van de Berg, W. J., van Meijgaard, E., Velicogna, I., and Wouters, B.: Partitioning Recent Greenland Mass Loss, Science, 326, 984–986, 2009.

Velicogna, I. and Wahr, J.: Acceleration of Greenland ice mass loss in spring 2004, Nature, 443, 329–331, 2006.

Yashayaev, I., Bersch, M., and van Aken, H. M.: Spreading of the Labrador Sea Water to the Irminger and Iceland basins, Geophys. Res. Lett., 34, L10602, doi:10.1029/2006gl028999, 2007.

Zuo, H., Mugford, R. I., Haines, K., and Smith, G. C.: Modelling Arctic Ocean Heat and Freshwater Budgets and their Variability: the Effect of Data Assimilation, Ocean Model., in press, 2011.

Zwally, H. J., Abdalati, W., Herring, T., Larson, K., Saba, J., and Steffen, K.: Surface melt-induced acceleration of Greenland ice-sheet flow, Science, 297, 218–222, 2002.

TCD
5, 1335–1364, 2011

Warming of waters in an East Greenland fjord prior to glacier retreat

P. Christoffersen et al.

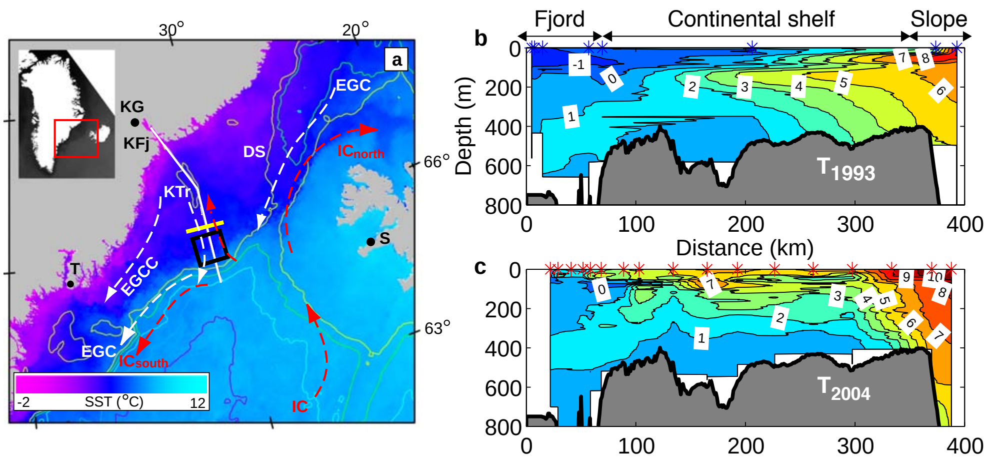

Fig. 1. (a) Map of central East Greenland and regions near Denmark Strait (DS). KG, KFj and KTr mark locations of Kangerlugssuaq Glacier, Kangerlugssuaq Fjord and Kangerlugssuaq Trough. White solid line shows hydrographic transect for the vertical sections shown in **(b)** (1993) and **(c)** (2004). Black box represents the area used to compute temperature and salinity at depth. The yellow line is a transect used to calculate variations in oceanic heat flux. Dashed arrows illustrate paths of the Irminger Current (IC), East Greenland Current (EGC) and East Greenland Coastal Current (EGCC). Colours illustrate whether currents are warm (red) or cold (white). Contours mark bathymetry in 500 m intervals and the background colour scheme shows sea-surface temperature in August 2004 from Oceancolor SST climatology. Black dots mark location of Tasiilaq (T) and Stykkisholmur (S). **(b)** Vertical section showing potential temperature of water masses in KFj and KTr in September 1993. **(c)** Same as **(b)**, but for observations in September 2004. The topographic overlay is the observed bathymetry in KFj and along KTr.

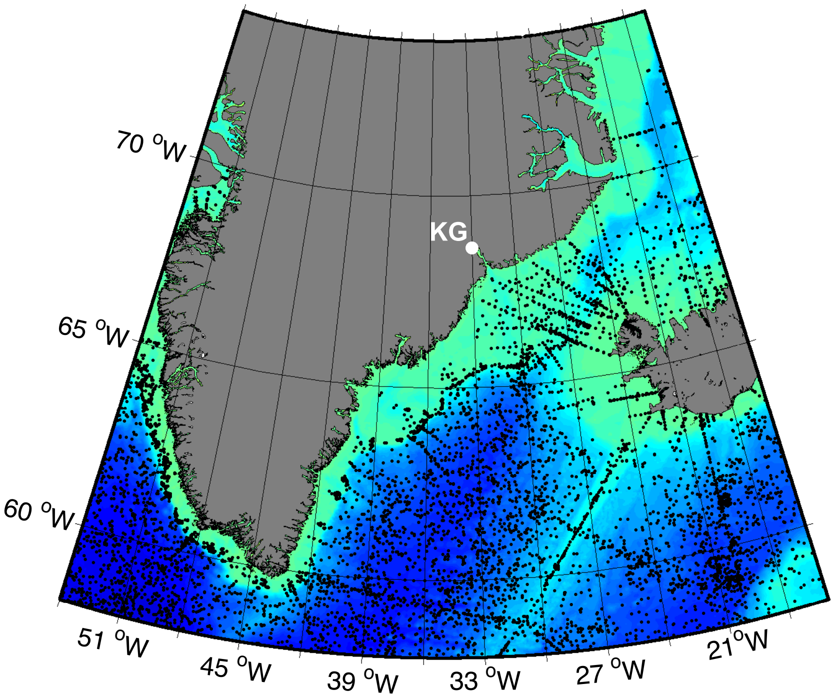

Fig. 2. Map of Greenland and the Irminger Sea with solid black dots showing location of in situ salinity and temperature measurements assimilated in the ocean reanalysis (see text for details). White dot marke location of KG.

TCD
5, 1335–1364, 2011

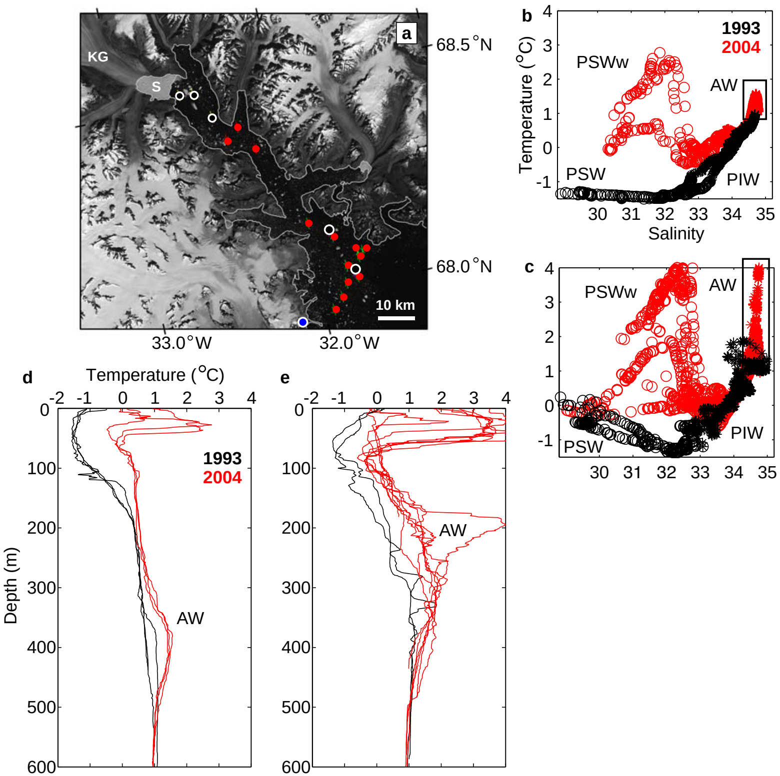

Fig. 3. (a) Landsat image showing KG and KFj on 16 August 2002. White circles show locations of CTD casts in 1993 and red dots show corresponding stations in 2004. Blue dot denotes the approximate location of Aputiteq. **(b)** Potential temperature and salinity from CTD data acquired in the upper central fjord (68.4° N, 32.2° W) in 1993 (black) and 2004 (red). Data from 0–100 m are marked open circles and deeper measurements are shown with asterisk. **(c)** Same as **(b)** but for data acquired at fjord mouth (68.1° N, 31.9° W). **(d)** Potential temperature from CTD casts in upper fjord in 1993 (black) and 2004 (red). **(e)** Same as **(d)**, but for CTD casts near fjord mouth.

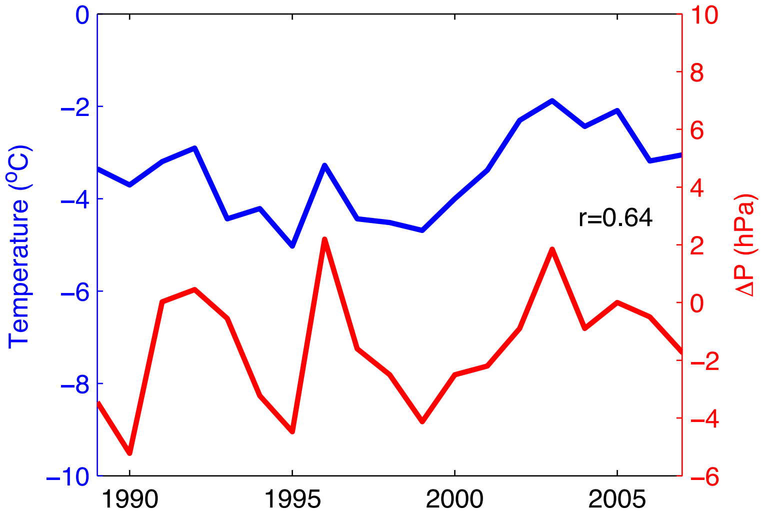

Fig. 4. Plot illustrating connection between mean annual air temperature meassured in Aputiteq (blue) and ΔP, which is the mean winter (December–March) difference between atmospheric pressure meassured in Stykkisholmur (Iceland) and Tasiilaq (Greenland). See text for details.

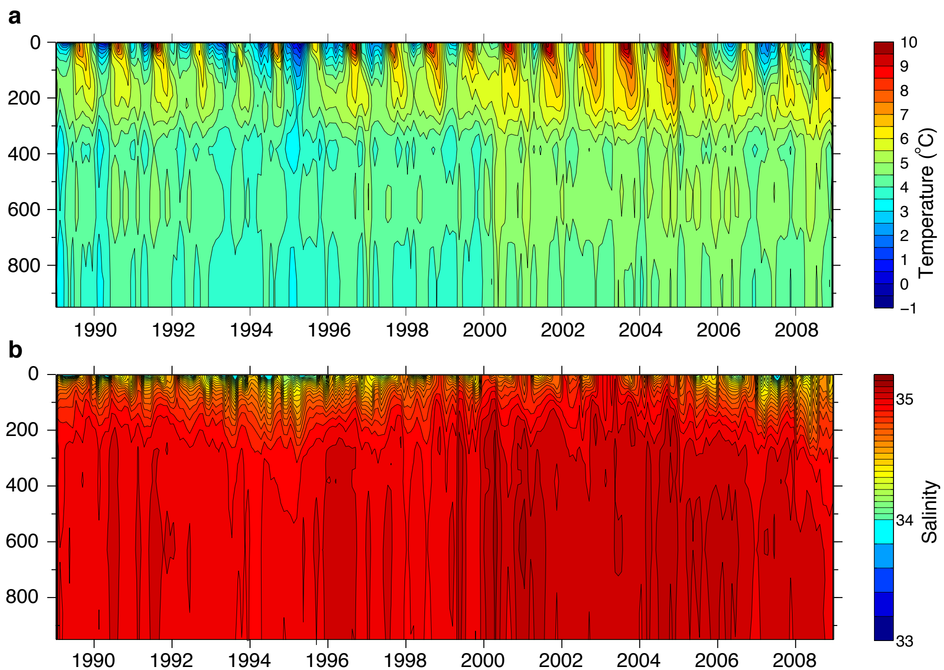

Fig. 5. Hovmøller diagrams showing potential temperature **(a)** and salinity **(b)** in ocean reanalysis. The data are averaged across black box shown in Fig. 1a.

TCD
5, 1335–1364, 2011

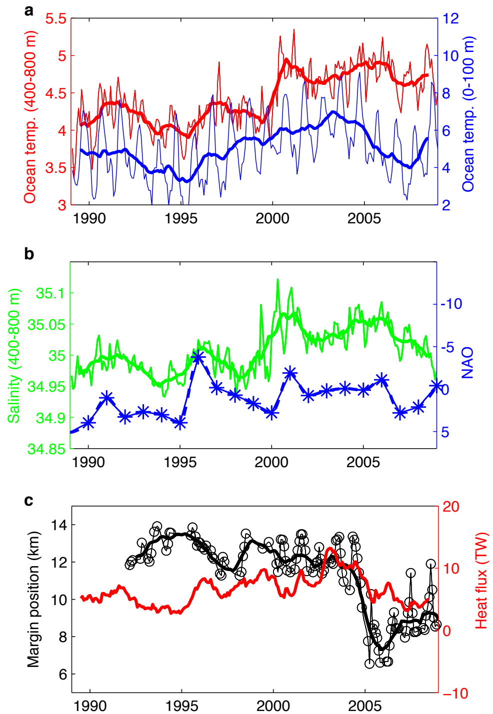

Fig. 6. **(a)** Time series of potential temperature as shown in Fig. 5, but averaged for 0–100 m (blue) and 400–800 m (red). Solid bold lines are 12-month-moving averages of monthly mean values. **(b)** Same as **(a)**, but for salinity at the 400–800 m level (green). Dashed blue line and asterisk show the extended NAO winter index. **(c)** Monthly margin positions of KG (black circles) derived from satellite imagery as described in text. Black bold line is the 12-month-moving average. The red line is the 12-month-moving average of heat flux calculated at transect shown in Fig. 1a and with reference to 0˚C. The heat flux is positive northward, which is into KTr and towards the coast.

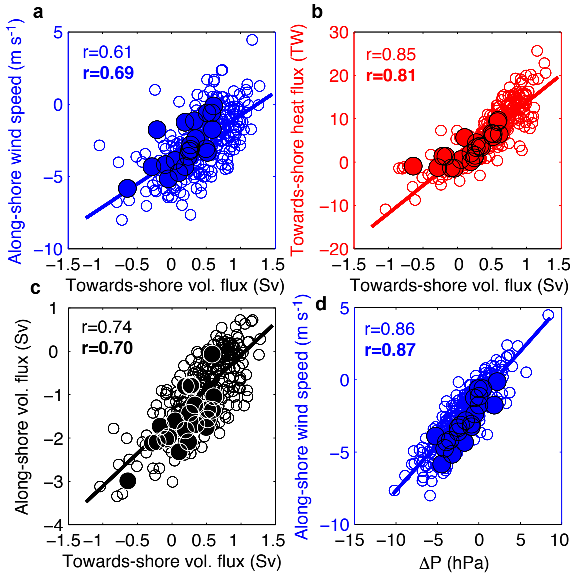

Fig. 7. Correlation plots from ocean reanalysis. **(a)** Scatter plot of mean monthly volume flux into and out of KTr (yellow line in Fig. 1a) and mean monthly speed of winds crossing Denmark Strait from the north at 66.3° N. North-flowing waters and wind yield positive values, which means that northerly winds have negative speed while transport into KTr and towards coast is positive. **(b)** Same as **(a)**, but with towards-shore volume flux compared against towards-shore heat flux calculated with reference to 0 °C. Heat flow is positive towards north, i.e. when it is directed into KTr and towards the coast. **(c)** Same as **(a)** and **(b)**, but with towards-shore volume flux plotted against the along-shore volume flux, i.e. flow of waters crossing the hydrographic transect shown by white line in Fig. 1a. This volume flux is positive when transport is from east to west. **(d)** Same as **(a)**, but with monthly wind speeds plotted against the Denmark Strait atmospheric pressure gradient, ΔP, derived from meteorological stations in Stykkisholmur and Tasiilaq (see text for details). Open circles and correlation coefficients shown in normal font represent monthly means while data averaged for winters months (December–March) are shown with filled solid circles and bold correlation coefficients.

TCD
5, 1335–1364, 2011

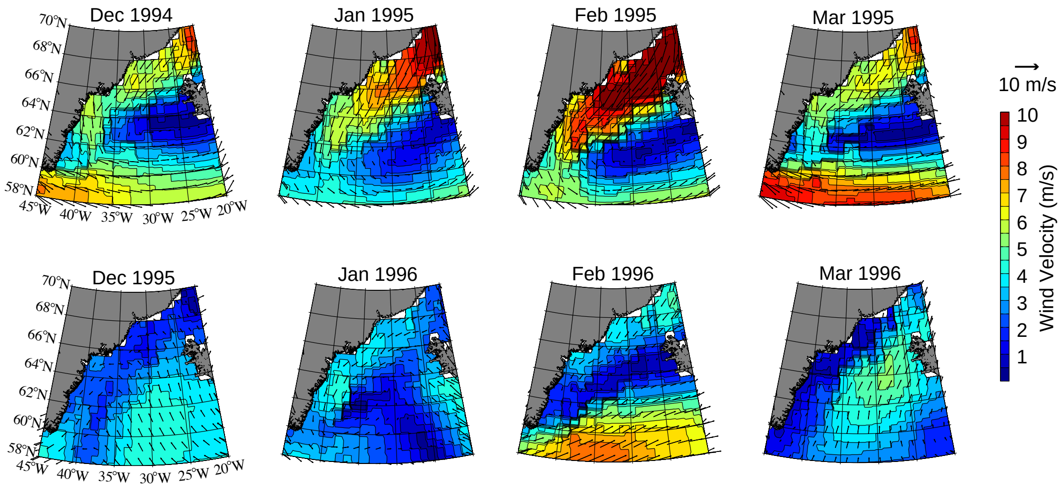

Fig. 8. Maps showing speed and direction of winds near the Denmark Strait during winters in 1994–1995 (top) and 1995–1996 (bottom). The data are from the atmospheric forcing set used to drive the ocean model (see text for details).

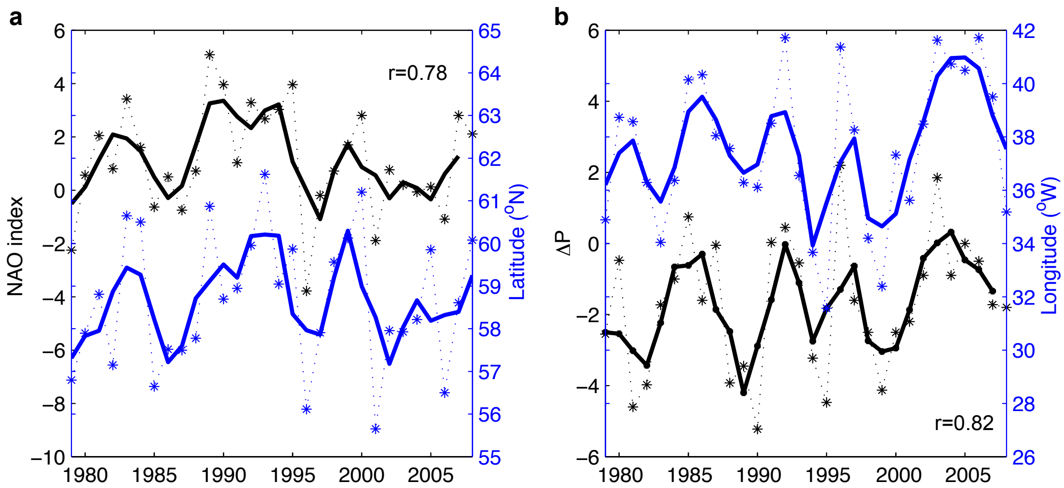

Fig. 9. **(a)** Plot showing the relationship between the mean latitude of the Icelandic Low (IL) during December-March and the extended (December–March) NAO winter index. **(b)** Same as **(a)** but showing the relationship between the longitude of the IL centre and ΔP. Solid lines show the 3-yr running means.